

Ultralong-range Cs-RbCs Rydberg molecules: non-adiabaticity of dipole moments

David Mellado-Alcedo,^{1,2} Alexander Guttridge,³ Simon L. Cornish,³ H. R. Sadeghpour,⁴ and Rosario González-Férez^{2,5,*}

¹*Departamento de Física, Universidad de Córdoba, 14071 Córdoba, Spain*

²*Departamento de Física Atómica, Molecular y Nuclear, Universidad de Granada, 18071 Granada, Spain*

³*Department of Physics, Durham University, South Road, Durham, DH1 3LE, United Kingdom*

⁴*ITAMP, Center for Astrophysics | Harvard & Smithsonian, Cambridge, Massachusetts 02138, USA*

⁵*Instituto Carlos I de Física Teórica y Computacional, Universidad de Granada, 18071 Granada, Spain*

(Dated: January 19, 2024)

We consider ultralong-range polyatomic Rydberg molecules formed by combining a Rydberg cesium atom and a ground-state RbCs molecule. We explore the regime where the charge-dipole interaction due to the Rydberg electron with the diatomic polar molecule couples the quantum defect Rydberg states $Cs(ns)$ to the nearest degenerate hydrogenic manifold. We consider polyatomic Rydberg molecules in states which are amenable to production in optical tweezers and study the influence of nonadiabatic coupling on the likelihood of their formation. The decay rates of the vibrational states reflect the interference signature of wave function spread in different coupled potential wells.

I. INTRODUCTION

The exaggerated properties of Rydberg atoms, such as their large spatial extents, high polarizabilities, and energies, make them an outstanding system for precisely probing interactions with the surrounding environment [1]. In an ultracold setting, a Rydberg atom, can couple to a ground state atom via the zero-range interaction due to Rydberg electron low-energy scattering from the ground state atom, or interact with another Rydberg atom via van der Waals or dipole-dipole forces [2]. A Rydberg atom can also couple to the permanent electric dipole moment of a polar molecule, via the electron-dipole interaction [3, 4]. For dipole moments below the Fermi-Teller critical dipole [5, 6], the electron-dipole interaction can produce a molecular bond capable of supporting bound rovibrational states. Such states are predicted to exist in a hybrid atom-molecule gas at ultracold temperatures. The prerequisite charge-dipole energy shift was recently observed for the first time in an ultracold hybrid system in an experiment with Rb Rydberg atoms and RbCs molecules trapped in separate optical tweezers [7].

In Rydberg atoms, core-electron scattering and polarization effects are significant for low angular momentum electronic states. Such states are energetically shifted from the degenerate manifold by means of the so-called quantum defects, which are the fingerprints that uniquely identify a Rydberg atom. The ns -states of cesium atom possess a peculiar quantum defect, such that $Cs(ns)$ states lie energetically near the corresponding hydrogenic $Cs(n-4, l \geq 4)$ states, which are nearly degenerate. Based on this proximity, trilobite Rydberg molecules Cs^*-Cs possessing sizable (~ 1 kD) permanent electric dipole moments, were observed for the spherically sym-

metric non-degenerate states $Cs(ns)$ [8–10]. Similarly, when one considers the interaction of a Cs Rydberg atom with a polar molecule, the $Cs(ns)$ quantum defect facilitates hybridization of the Rydberg states $Cs(ns)$ and $Cs(n-4, l \geq 4)$, which is mediated by the charge-dipole interaction [11]. As a consequence, the optimal scheme for the realization of the ultralong-range triatomic Rydberg molecules [11], based on this resonant coupling, also benefits from the fact that the diatomic molecule is in the rotational ground state.

Here, we provide a thorough theoretical study of the shift and formation of the triatomic molecule (TriMol) $Cs(ns)$ -RbCs. We first review the basic theory of the ultralong-range triatomic Rydberg molecules in Sec. II. In Sec. III, we consider two experimental protocols, corresponding to holding the atom and molecule in the same or separate optical tweezers, and present the results for selected potential energy curves (PEC) of this TriMol and their vibrational bound states. We analyze the impact on the energy shifts of the scattering of the low-energy Rydberg electron from RbCs. Inspired by previous studies on non-adiabatic effects on Rydberg systems [12, 13], we also explore the role played by the avoided crossings, and provide the Franck-Condon factors for excitation from the atomic ground state. The paper is concluded in Sec. IV.

II. THE BORN-OPPENHEIMER HAMILTONIAN

We consider a TriMol formed by a Rydberg atom and a heteronuclear diatomic molecule in the electronic and rovibrational ground state. The ground state diatomic molecule is described within the Born-Oppenheimer (BO) and rigid rotor approximations, whereas the Rydberg atom is described as a single-electron system. In this framework, the adiabatic Hamiltonian of the Ryd-

* rogonzal@ugr.es

berg TriMol is

$$H = H_A + H_{\text{mol}} + H_{\text{int}}, \quad (1)$$

where H_A represents the single-electron Hamiltonian describing the Rydberg atom

$$H_A = -\frac{\hbar^2}{2m_e} \nabla_r^2 + V_l(r), \quad (2)$$

where $V_l(r)$ is an l -dependent nonlocal model potential [14], with l the angular momentum of the Rydberg electron. The rigid rotor Hamiltonian describing the molecule is $H_{\text{mol}} = B\mathbf{N}^2$ with B the rotational constant, and \mathbf{N} the rotational angular momentum.

In this ultracold hybrid system, where the interactions are long-range, the Hamiltonian between the Rydberg atom and the molecule becomes

$$H_{\text{int}} = -\mathbf{d} \cdot \mathbf{F}_{\text{ryd}}(\mathbf{R}, \mathbf{r}) + 2\pi a_S(k)\delta(\mathbf{r} - \mathbf{R}), \quad (3)$$

where the first term represents the interaction of the Rydberg electron and ionic core with the RbCs permanent electric dipole moment \mathbf{d} . The electric field $\mathbf{F}_{\text{ryd}}(\mathbf{R}, \mathbf{r})$ due to the Rydberg electron and the ion at the position of the diatomic molecule, \mathbf{R} , is

$$\mathbf{F}_{\text{ryd}}(\mathbf{R}, \mathbf{r}) = \frac{e}{4\pi\epsilon_0} \left(\frac{\mathbf{R}}{R^3} + \frac{\mathbf{r} - \mathbf{R}}{|\mathbf{r} - \mathbf{R}|^3} \right), \quad (4)$$

where e is the electron charge and \mathbf{r} is the position of the Rydberg electron. Note that the center of the coordinate system is located at the position of the ionic core, Cs^+ . In this work, we consider the RbCs molecule with a rotational constant of $B = 0.490$ GHz [15] in the electronic and vibrational ground state with an electric dipole moment of $d = 1.225$ D [16], below the Fermi-Teller critical dipole, $d_{cr} = 1.639$ D [5, 6]. The subcritical dipole moment of RbCs ensures that the electron does not bind to the molecule.

The second term in Eq. (3) represents the scattering of the low-energy, nearly-free electron from the diatomic molecule. This is approximated by the Fermi pseudopotential [17, 18], assuming that only the $L = 0$ (S -wave) scattering partial wave contributes to the collision. The S -wave scattering length, $a_S(k) = -\tan(\delta_S(k))/k$, with $\delta_S(k)$ as the $L = 0$ scattering phase shift, and k the electron wave number, is approximated by a constant value $a_S = 1/\sqrt{2E_A}$ [19], where E_A is the electron affinity of RbCs.

For the numerical description of this system, we fix the center of the laboratory fixed frame at the ionic core Cs^+ , and the diatomic molecule is situated along the Z axis. The Schrödinger equation associated with the Hamiltonian (1) is solved for several values of the interspecies separation R . Hence, the potential energy surfaces of the Rydberg molecule Cs-RbCs reduce to curves, which only depend on R . To solve this Schrödinger equation, we perform a basis set expansion in terms of the coupled

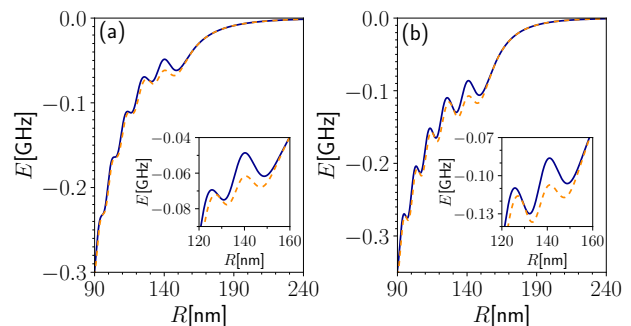


FIG. 1. Adiabatic electronic potential curves of the Cs-RbCs Rydberg molecule with $M_J = 0$. (a) for Cs(41p)-RbCs ($N = 0$), (b) for Cs(40d)-RbCs ($N = 0$). Blue solid lines include the electron scattering with RbCs and orange dashed lines represent the curves with this term neglected. In panels (a) and (b), the zero energies are set to the Rydberg energies $E(\text{Cs}(41p))$ and $E(\text{Cs}(40d))$, respectively.

molecular basis [4]

$$\Psi(\mathbf{r}, \Omega; R) = \sum_{n,l,N,J} C_{n,l,N}^J(R) \Psi_{nl,N}^{JM_J}(\mathbf{r}, \Omega), \quad (5)$$

where $|l - N| \leq J \leq l + N$, and

$$\Psi_{nl,N}^{JM_J}(\mathbf{r}, \Omega) = \sum_{m_l, M_N} \langle lm_l N M_N | J M_J \rangle Y_{N M_N}(\Omega) \psi_{nlm_l}(\mathbf{r}) \quad (6)$$

with $\langle lm_l N M_N | J M_J \rangle$ the Clebsch-Gordan coefficients, $J = |l - N|, \dots, l + N$, and $M_J = -J, \dots, J$. $\psi_{nlm_l}(\mathbf{r})$ is the Rydberg electron wave function with n , l and m_l the principal, orbital and magnetic quantum numbers, respectively, and $Y_{N M_N}(\Omega)$ the field-free rotational wave function of the diatomic molecule, whose rotation is described with the Euler angles $\Omega = (\theta, \phi)$. The total angular momentum of the Rydberg molecule, excluding an overall rotation, is given by $\mathbf{J} = \mathbf{l} + \mathbf{N}$, where \mathbf{l} is the orbital angular momentum of the electron and \mathbf{N} the rotational angular momentum of the diatomic molecule. We include rotational excitations in RbCs ($N \leq 5$), the Cs(ns, np, nd, nf) quantum defects, the degenerate manifold, and investigate electronic states of the TriMol with $M_J = 0$.

III. RESULTS

A. Zero-range electron-molecule scattering

We first quantify the effect of electron-molecule scattering on the adiabatic electronic potentials. In the collision of an electron with RbCs($X^1\Sigma$) negative ions could be formed, and the measured electron affinity of RbCs is $E_A = 0.478 \pm 0.020$ eV [20]. *Ab initio* calculations of the low-energy electron-molecule scattering length are notoriously difficult. We therefore estimate the magnitude of the scattering length using $a_S = (2E_A)^{-1/2} \sim$

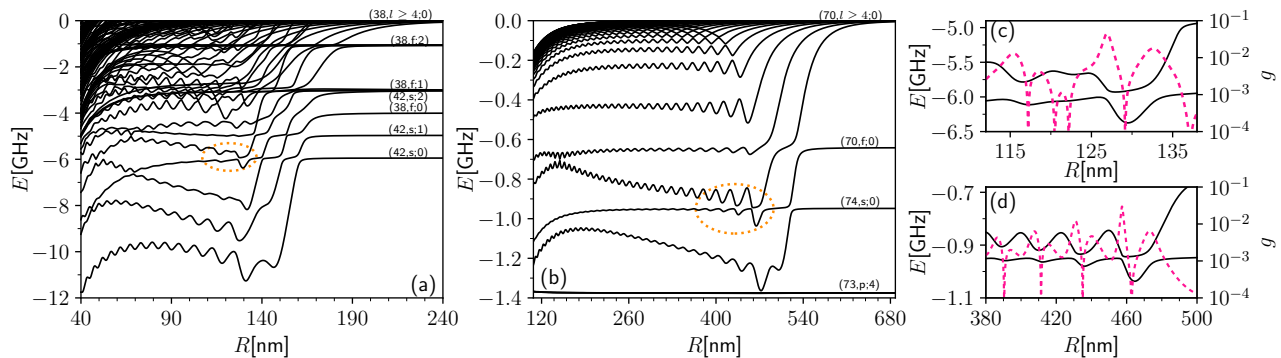


FIG. 2. For the Cs-RbCs Rydberg molecule, adiabatic electronic potential energy curves for $M_J = 0$ evolving from (a) the Rydberg states Cs($n = 38, l \geq 4$) and the RbCs in the ground state, Cs($42s$)-RbCs($N \leq 2$) and Cs($38f$)-RbCs($N \leq 2$) and (b) the Rydberg state Cs($n = 70, l \geq 4$) and the RbCs in the ground state, Cs($70f$)-RbCs($N = 0$), Cs($74s$)-RbCs($N = 0$) and Cs($73p$)-RbCs($N = 4$). The labels ($n, l; N$) are used to identify the Rydberg potentials Cs(nl)-RbCs(N). In panels (c) and (d), the left axis shows potential curves (black solid lines) and the right axis shows the Landau-Zener coupling $g = |\langle \Psi_i | \frac{\partial}{\partial R} | \Psi_j \rangle|$ (magenta dashed lines) for the avoided crossings encircled in panels (a) and (b), respectively.

$5.34 a_0$. The existence of an E_A for RbCs implies the sign of the scattering length is positive. We use a k -independent scattering length in the S -wave Fermi-pseudopotential Eq. (3). The effect of this interaction is illustrated in Fig. 1 for the adiabatic potentials of Cs($41p$)-RbCs($N = 0$) and Cs($40d$)-RbCs($N = 0$), which have been computed with (blue solid lines) and without (orange dashed lines) the pseudopotential in Eq. (3). Because $a_S > 0$, the effect of the Fermi-pseudopotential is to blue-shift the energies from those obtained with only the charge-dipole interactions in Eq. (4). We find, as expected, that the largest difference between these potentials is near the last maximum of the Rydberg wave function where we calculate a difference of around 48.6 MHz between the two curves.

B. Cs*-RbCs Rydberg polyatomic molecules

We consider two possible experimental protocols to create ultralong range polyatomic Rydberg molecules. Firstly, the ground state Cs atom and the RbCs molecule are prepared in the motional ground state of two separate optical tweezers, as demonstrated for Rb in Ref. [7]. Then, the optical tweezers are merged, ideally achieving a high occupation of the ground state of the relative motion of Cs and RbCs. Finally, the Cs atom is excited to a Rydberg state so that RbCs lies within the electron orbit. Within the same optical tweezer, the spatial separation between the atom and molecule should be smaller might be smaller than 200 nm, and the condition of lying within the orbit could be satisfied with a two-photon excitation to the Cs($42s$) Rydberg state. An alternative route is to leave the atom and molecule in their separate optical tweezers and to then excite the Cs atom. In this case, the spatial separation between the centers of the tweezers of $\lambda/2 \sim 500$ nm is achievable, and a higher principal quantum number for the Rydberg excitation is required.

In this work, we take Cs($74s$) as an example to illustrate this second option.

The electronic structures of the TriMol Cs($42s$)-RbCs($N = 0$) and Cs($74s$)-RbCs($N = 0$) are presented in Figs. 2 (a) and (b), respectively. Due to the peculiar quantum defect of Cs(ns), the adiabatic potential curve for the TriMol Cs(ns)-RbCs($N = 0$) lies among those electronic states evolving from the Rydberg degenerate manifold Cs($n - 4, l \geq 4$) combined with RbCs($N = 0$). As a consequence, the electronic spectrum of these TriMol Cs*-RbCs is characterized by numerous avoided crossings, as observed in panels (a) and (b) of Fig. 2. Furthermore, because of the small RbCs rotational constant, the adiabatic potentials of the electronic states Cs($42s$)-RbCs(N) with $N \leq 2$, also become immersed among those evolving from Cs($n = 38, l \geq 4$)-RbCs($N = 0$), creating a highly complex spectrum.

The experimental observation of a TriMol requires the formation of a bound vibrational state in one of these electronic potentials in Fig. 2, which would be heralded by the appearance of a redshifted feature in the Cs Rydberg spectrum. In the avoided crossings marked in Figs. 2 (a) and (b) the coupling between neighboring electronic states is not negligible and provokes the predissociation of the bound vibrational states. In these regions the Born-Oppenheimer approximation breaks down, and the total wave function can be expressed as

$$\Phi(\mathbf{r}, \Omega, R) = \sum_{i=d,u} \Psi_i(\mathbf{r}, \Omega; R) \frac{\chi^i(R)}{R}, \quad (7)$$

where $\Psi_i(\mathbf{r}, \Omega; R)$ is the eigenfunction of the Hamiltonian (1) and is given by Eq. (5), and the index $i = d, u$ indicates the potentials down and up, respectively. The reduced vibrational wave functions $\chi^i(R)$ satisfy the fol-

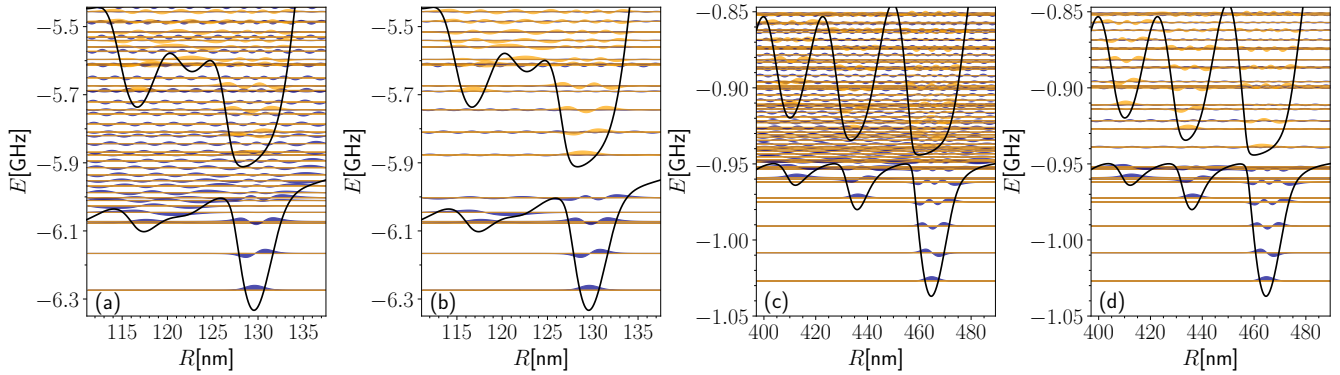


FIG. 3. For the electronic states Cs(42s)-RbCs($N = 2$) and Cs(38f)-RbCs($N = 1$) of the TriMol encircled in Fig. 2 (a), eigenenergies and their vibrational wave functions obtained from (a) the coupled Schrödinger equation (8) and (b) after stabilization technique is applied. Panels (c) and (d) show similar results for the lowest Cs($n = 70, l > 3$)-RbCs($N = 0$) and Cs(70f)-RbCs($N = 0$) potentials encircled in Fig. 2 (b). The vibrational wave functions are shifted from their corresponding energies and rescaled for better visibility, and the components $\chi^d(R)$ and $\chi^u(R)$ are plotted in blue and yellow, respectively.

lowing coupled Schrödinger equation [21]

$$\begin{pmatrix} T + V_d + \mathcal{A}_{dd} & \mathcal{A}_{du} \\ \mathcal{A}_{ud} & T + V_u + \mathcal{A}_{uu} \end{pmatrix} \begin{pmatrix} \chi^d \\ \chi^u \end{pmatrix} = E \begin{pmatrix} \chi^d \\ \chi^u \end{pmatrix}, \quad (8)$$

with $T = -\frac{\hbar^2}{2m} \frac{d^2}{dR^2}$ the reduced kinetic energy and m the reduced mass of the Rydberg TriMol. The coupling terms are $\mathcal{A}_{ij} = \langle \Psi_i | T | \Psi_j \rangle - \frac{\hbar^2}{m} \langle \Psi_i | \frac{d}{dR} | \Psi_j \rangle \frac{d}{dR}$, whereas the potentials $V_i = \langle \Psi_i | H | \Psi_i \rangle$ are the eigenvalues of the adiabatic Hamiltonian (1), with $i, j = d, u$. Note that equation (8) is only valid for bound states of the Rydberg molecule with zero rotational angular momentum.

The states of the coupled potential energy curves Cs(42s)-RbCs($N = 2$) and Cs(38f)-RbCs($N = 1$) computed within the non-adiabatic Schrödinger equation (8), are presented in Fig. 3 (a) together their wave functions. The contributions to the wave functions from the potentials down and up, i.e., $\chi^d(R)$ and $\chi^u(R)$, respectively, are plotted in different colors. To determine which states are truly bound, we solve the coupled Schrödinger Eq. (8) varying the lower limit of the radial coordinate and use the stabilization method [22]. The bound states are those levels whose energy could be considered independent of R_{min} , and they are presented in panel (b) of Fig. 3. For the sake of completeness, the corresponding stabilization diagram of the energies in Fig. 3 (a) is shown in Fig. 8 of the appendix. A similar study is done for the electronic potential evolving from Cs(70f)-RbCs($N = 0$) taking into account non-adiabatic coupling to the upper potential evolving from Cs(70, $l \geq 4$)-RbCs($N = 0$), all eigenstates for a fixed radial range are presented in Fig. 3 (c). Whereas the truly bound ones, obtained after the stabilization analysis is applied, are shown in Fig. 3 (d).

The broad avoided crossings hardly influence the deeply bound states in the outer well potential, and their wave functions are dominated by the components in the lower potential, i.e., $\mathcal{W}_i^d \sim 1$, and see Eq. (A5) for the weights, as the contribution from the upper potential is

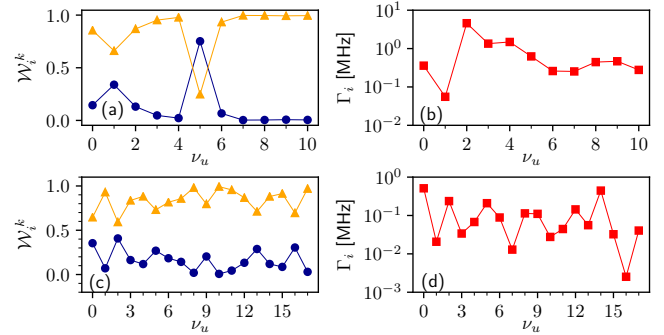


FIG. 4. For the vibrational states in the upper potentials in Figs. 3 (b) and (d), panels (a) and (c) present weights, as defined in Eq. (A5), of the vibrational wave function in the lower and upper potentials i.e., \mathcal{W}_i^d (blue circles) and \mathcal{W}_i^u (yellow triangles), as a function of the vibrational quantum number in these upper potentials; (b) and (d) present decay rates as defined in Eq. (A7) as a function of the vibrational quantum number in these upper potentials, respectively.

very small. In contrast, the impact is significant for the states lying on the upper potential. Their wave functions are dominated by the contribution from this upper potential, but still possess a significant weight from lower one as shown in Fig. 4 (a) and (c). The three lowest states within the right well of Cs(38f)-RbCs($N = 1$) possess the largest mixing, together with the $\nu_u = 5$ state, which due to the spatial extension of its wave function shows the highest coupling to the lower potential. Note that for the rightmost well in the upper potential in Fig. 3 (c), which evolves from Cs(70, $l \geq 4$)-RbCs($N = 0$), we encounter three states associated with the first excited vibrational state, i.e., the part of their wave functions on the upper potential possess a node. For two of the states, the contributions from the lower potential to their total wave functions, see Eq. (A5), are larger than 73%, whereas for third state, it is 47%. However, they are not bounded

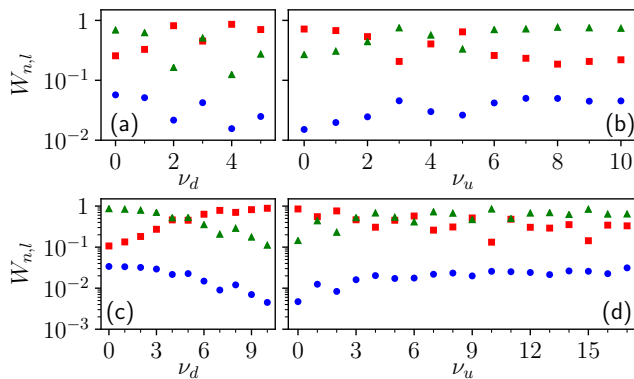


FIG. 5. Integrated weights of the Rydberg l -partial waves in the electronic wave function, $W_{n,l=0}$ (red squares), $W_{n,l=3}$ (blue dots) and $\sum_{l \neq 0,3} W_{n,l}$ (green triangles), see Eq. (A2), for the bound states within the lower and upper potential energy curves (a) and (b), respectively, in Fig. 3 (b). Panels (c) and (d) show analogous results for the bound states in the lower and upper potentials in Fig. 3 (d).

because their energies are not stable as the lower limit of the radial coordinate is changed when solving the coupled Schrödinger equation in the stabilization diagram.

To illustrate the coupling induced at the avoided crossings, we have computed the nonadiabatic decay rates Eq. (A7) of the bound states in the upper potential to the continuum states. The results for the vibrational states within the Cs(38*f*)-RbCs($N = 1$) and the lowest electronic state from the degenerate manifold Cs(70, $l \geq 4$)-RbCs($N = 0$) are shown in Figs. 4 (b) and (d), respectively. The trend in the decay rate for the vibrational states in Fig. 3 (b) is as expected; the higher vibrational states away from the avoided crossing region decay more slowly than the states near the crossing. For those states located in a potential well, the nodal structure of the vibrational wave function gives rise to the oscillatory behaviour of the decay rate. For the vibrational states in the upper potential in Fig. 3 (d), the oscillation in the decay rate is a reflection of the interference of the wave function spread in the three wells.

For the vibrational bound states within the lower and upper potentials in Fig. 3 (b) and (d), we have also analyzed the hybridization of the Rydberg partial waves due to the charge-dipole interaction. The weights of the s and f partial waves, and the sum of the rest, see Eq. (A6), to the wave functions of the vibrational bound states of the Cs(42*s*)-RbCs($N = 2$) and Cs(38*f*)-RbCs($N = 1$) potentials are shown in Fig. 5 (a) and (b), respectively. The s -wave is dominant only for those bound states close to the avoided crossing region, i. e., the high (low)-lying states in the lower (upper) potential. This is due to the avoided crossing with the potentials Cs(42*s*)-RbCs($N = 0$) and Cs(42*s*)-RbCs($N = 1$) at larger internuclear separations. For all states, the Rydberg partial waves with $l \geq 3$ possess significant weights, having the largest contribution for excited states on the upper potentials. These results

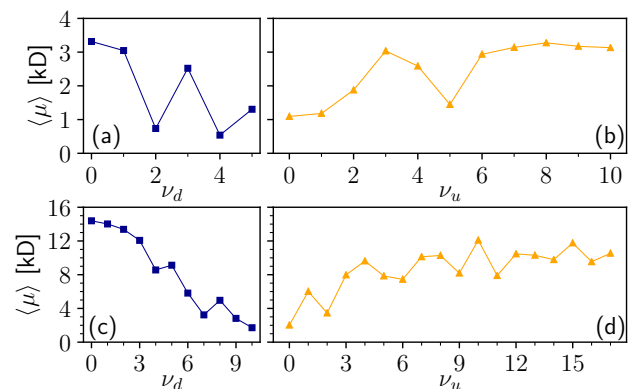


FIG. 6. For the bound states within the lower and upper potentials in Fig. 3 (b), panels (a) and (b) show the permanent electric dipole moment defined in Eq. (A4), respectively. Panels (c) and (d) show analogous results for the bound states in the lower and upper potentials in Fig. 3 (d). The sudden decrease in the dipole moment for the vibrational quantum numbers $\nu_d = 2$ and 4 in panel (a) is because these states are localized in the inner well of the down potential and, therefore, being less affected by the avoided crossing in Fig. 3 (b).

indicate a significant hybridization of the Rydberg partial waves, giving rise to huge permanent electric dipole moments (\sim kD), as illustrated in Fig. 6 (a) and (b).

Figures 5 (c) and (d) present the Rydberg partial waves contributions to the vibrational states in the Cs(70*f*)-RbCs($N = 0$) and Cs(70, $l \geq 4$)-RbCs($N = 0$) potentials, respectively. We encounter a strong mixing, indeed, they do not inherit a dominant f -wave character from the potential correlating to the Cs(70*f*)-RbCs($N = 0$) dissociation limit. Again, the contribution of the s -partial wave is dominant for those states close to the avoided crossing region, i. e., the highest- and lowest-lying levels in the lower and upper potentials in Fig. 3 (d), respectively. As a consequence, they all possess massive electric dipole moments as presented in Fig. 6 (c) and (d).

For the vibrational bound states within the lower potential energy curve, we have computed the weighted Franck-Condon factors in Fig. 7, taking the Rabi frequency for the two-photon Rydberg excitation to the ns Rydberg states as $\Omega_{n,s} = 1$. The Franck-Condon factors strongly depend on the nodal structure of the vibrational wave function. For the Cs(42*s*)-RbCs($N = 2$) potential, the lowest lying state of the left well possesses the largest Franck-Condon factor, which is also due to its significant s -wave and $N = 0$ contributions to the wave function. For the Cs(70*f*)-RbCs($N = 0$) potential, we encounter that excited states possess larger Franck-Condon factors, for instance, the lowest lying states within the leftmost potential well, and the second excited state in the central well. This could be due to the larger contribution of the Rydberg s partial wave to their wave function. These results indicate that in both cases, there exists several vibrational bound states that could be used for the photoassociation of these TriMols.

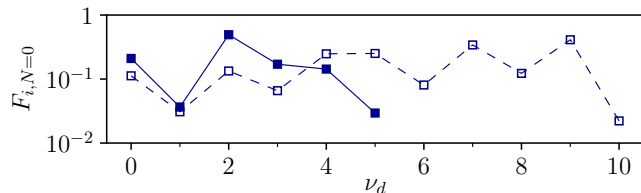


FIG. 7. Weighted Franck-Condon factors with $l = 0$ Rydberg partial wave and $N = 0$, assuming the Rabi frequency for the corresponding two-photon Rydberg excitation $\Omega_{ns} = 1$, see Eq. (A9), to the bound states within the lower potential energy curves Cs($42s$)-RbCs($N = 2$) in Fig. 3 (b) (filled squares), and Cs($70f$)-RbCs($N = 0$) in Fig. 3 (d) (empty squares).

IV. CONCLUDING REMARKS AND OUTLOOK

We have investigated triatomic ultralong-range Rydberg molecules formed by a Rydberg cesium atom and a RbCs diatomic molecule. Our theoretical description includes the charge-dipole interaction arising from the coupling of the permanent dipole moment of RbCs with the electric field produced by the Rydberg electron and core, and the S -wave scattering of the slow Rydberg electron from the molecule. Due to the peculiar quantum defects of Cs, the charge-dipole interaction induces a coupling between the s -wave quantum defect Rydberg states and the nearest degenerate hydrogenic manifold, as both states are combined with RbCs in its rotational ground state.

Assuming that the Rydberg atom and the diatomic molecule are confined in optical tweezers [7], we focus on the Rydberg molecules evolving from Cs($42s$)-RbCs($N = 0$) and Cs($74s$)-RbCs($N = 0$), whose interspecies separations correspond to the two possible scenarios with Cs and RbCs being in the same tweezer or in separate ones, respectively. For these electronic states, we have explored the role played by the non-adiabatic coupling near the avoided crossings, their main features and vibrational structure. In both cases, we have identified vibrational bound states with large Franck-Condon factors, that could be used to form the polyatomic Rydberg molecules.

Near resonant coupling between Rydberg states and molecular rotation induces long-range dipole-dipole interactions. Charge-dipole coupling induces gigantic shifts and permanent polyatomic molecular dipole moments. These state-specific interactions can be utilized to perform conditional and nondestructive readout of molecular state [23–28]. In addition, quantum gates between molecules could be implemented using the Rydberg states of Cs as facilitators [27, 28]. A number of different ultracold alkali molecules containing Cs atoms have been successfully produced in a variety of settings. For instance, production of molecules in the absolute ground state has been achieved for LiCs using photoassociation [29], NaCs using magnetoassociation in optical

TABLE I. Transitions of the Cs atom and diatomic molecules formed from Cs and energy differences of these transitions that could be used to create quantum gates.

Cesium Rydberg Transition	Molecule and Rotational Transition	Energy difference [MHz]
$95S_{1/2} \rightarrow 92P_{3/2}$	LiCs, $N = 1 \rightarrow 2$	2.3
$47D_{5/2} \rightarrow 48P_{3/2}$	NaCs, $N = 1 \rightarrow 2$	4.3
$118D_{3/2} \rightarrow 115P_{1/2}$	KCs, $N = 0 \rightarrow 1$	0.4
$85D_{3/2} \rightarrow 86P_{3/2}$	RbCs, $N = 0 \rightarrow 1$	0.6

tweezers [30] and bulk gases [31], and RbCs molecules have been produced in bulk gases [16, 32] and optical tweezers [7]. In addition, there are good prospects for reaching the ground state of ultracold KCs [33]. For all these polar alkali dimers, we present in Table I a selection of the pairs of rotational levels and of Rydberg states in Cs, that could be used for this near-resonant interaction, along with the energy difference between these transitions. These energy splittings could be brought closer to resonance by applying electric or magnetic fields to smoothly tune the Rydberg states.

The precision tunability of Rydberg atoms and the stability of molecular dipoles combine to induce anisotropic long-range interactions with new scales and functionality. This hybrid atom-molecule system holds potential for investigation of an entire class of quantum processes, including quantum magnetization and quantum simulations.

ACKNOWLEDGMENTS

D.M.A. and R.G.F. gratefully acknowledge financial support by the Spanish projects PID2020-113390GB-I00 (MICIN), PY20.00082 (Junta de Andalucía), and A-FQM-52-UGR20 (ERDF-University of Granada) and the Andalusian research group FQM-207. A.G and S.L.C. acknowledge support from the UK Engineering and Physical Sciences Research Council (EPSRC) Grants EP/P01058X/1, EP/V047302/1, and EP/W00299X/1, UK Research and Innovation (UKRI) Frontier Research Grant EP/X023354/1, the Royal Society, and Durham University. H.R.S. acknowledges support at ITAMP through a grant by the NSF.

Appendix A: Expressions

In this appendix, we describe the quantities analyzed to get a better physical insight of the features of the TriMol. To illustrate the induced coupling due to the charge-dipole interaction, we compute the weight of a certain partial wave of the Rydberg electron in a k -electronic

state of the TriMol wave function (5), which is given by

$$C_{n,l}(R) = \sum_{N,J} |C_{n,l,N}^J(R)|^2, \quad (\text{A1})$$

where the sum in J is for $|l - N| \leq J \leq l + N$, and satisfies $\sum_{n,l} C_{n,l}(R) = 1$. For a vibrational bound state, we define the weight of this Rydberg-electron partial wave as

$$W_{n,l}^\nu = \int (\chi(R))^* C_{n,l}(R) \chi(R) dR, \quad (\text{A2})$$

and $\sum_{n,l} W_{n,l}^k = 1$. Note that $\chi(R)$ represents the reduced wave function of a vibrational state, and satisfies the following Schrödinger equation

$$\left[-\frac{\hbar^2}{2m} \frac{d^2}{dR^2} + V(R) \right] \chi(R) = E \chi(R) \quad (\text{A3})$$

with m being the reduced mass of the TriMol, and $V(R)$ the corresponding adiabatic potential energy curve.

We also estimate the electric dipole moment of this vibrational state by

$$\langle \mu \rangle = \int (\chi(R))^* D_{ryd}(R) \chi(R) dR, \quad (\text{A4})$$

with the R -dependent electric dipole moment given by

$$D_{ryd}(R) = e \int \Psi^*(\mathbf{r}, \Omega; R) r \cos \theta_e \Psi(\mathbf{r}, \Omega; R) d^3 r d\Omega,$$

where θ_e is the polar angle of the Rydberg electron. This integral is non-zero if there are partial waves with different parity, i.e., $\Delta l = \pm 1$, contributing to the wave function (5).

For a bound state in the coupled electronic potentials, we define the weight of the wave function in the potentials down and up as

$$W_i^k = \int |\chi_i^k(R)|^2 dR \quad (\text{A5})$$

where $\chi_i^k(R)$ represents the part of reduced wave function in the k -potential with $k = d, u$, and i identifies the vibrational states. For all bound states, it holds $W_i^d + W_i^u = 1$. For each of these bound states, the weights of the Rydberg-electron wave function are defined, respectively, as

$$W_{n,l} = \sum_{k=d,u} W_{n,l}^k. \quad (\text{A6})$$

The non-adiabatic decay rates due to coupling near the avoided crossings are expressed as [13]

$$\Gamma_i = \frac{2\pi}{\hbar} |\langle \chi_i^d | A_{du} | \chi_j^u \rangle|^2 \quad (\text{A7})$$

where $A_{du} = \langle \Psi_d | T | \Psi_u \rangle - \frac{\hbar^2}{m} \langle \Psi_d | \frac{d}{dR} | \Psi_u \rangle \frac{d}{dR}$, with χ_j^u is the vibrational wave function of a bound state in the upper potential, and χ_i^d is the the continuum wave function in the lower potential at the same energy. Note that the scattering state χ_i^d is energy normalized, whereas computationally it is L^2 normalized. A numerical way to obtain these energy normalized wave functions is described in Ref. [34].

In the coupled picture, the electronic dipole moment of a bound state is

$$\langle i | \mu | i \rangle = \int (\chi_i^{k_1}(R))^* D_{ryd}^{k_1, k_1}(R) \chi_i^{k_1}(R) dR, \quad (\text{A8})$$

with the dipole moment of the electronic state k_1 , with $k_1 = d, u$, given by

$$D_{ryd}^{k_1, k_1}(R) = e \int \Psi_{k_1}^*(\mathbf{r}, \Omega; R) r \cos \theta_e \Psi_{k_1}(\mathbf{r}, \Omega; R) d^3 r d\Omega.$$

To estimate the probability of forming these Rydberg molecules by a two photon transition, we compute the Franck-Condon factors weighted with $l = 0$ Rydberg partial wave,

$$F_{i,N} = \sum_{k=d,u} \int (\chi_i^k(R))^* \Omega_{ns} C_{n,l=0,N}^{J,k}(R) \psi_{scat}(R) R dR \quad (\text{A9})$$

with $\psi_{scat}(R)$ being the scattering wave function of the initial open channel and $\chi_i^k(R)$ the vibrational wave function of the final potential energy curve of the TriMol, and Ω_{ns} the Rabi frequency for a two-photon Rydberg excitation to the ns state, which was taken equal to 1 in our calculations. We are assuming that the process is dominated by a single ns Rydberg state, i.e., there is no significant admixture of different principle quantum numbers, then we can drop the sum over n .

In Fig. 8, we present the stabilization diagram of the electronic potentials of Cs-RbCs shown in Fig. 3 (a). We have solved the Schrödinger equation (8) by using different discretization boxes for R and modifying their lower limit R_{min} [34]. Those level whose energy could be considered independent of R_{min} in Fig. 8 are the states that are truly bound within these potentials, and are shown in panel (b) of Fig. 3.

-
- [1] C. S. Adams, J. D. Pritchard, and J. P. Shaffer, *J. Phys. B: At. Mol. Opt. Phys.* **53**, 012002 (2019).
 [2] J. P. Shaffer, S. T. Rittenhouse, and H. R. Sadeghpour, *Nat. Commun.* **9**, 1965 (2018).
 [3] S. T. Rittenhouse and H. R. Sadeghpour,

- Phys. Rev. Lett.* **104**, 243002 (2010).
 [4] R. González-Férez, H. R. Sadeghpour, and P. Schmelcher, *New J. Phys.* **17**, 013021 (2015).
 [5] E. Fermi and E. Teller, *Phys. Rev.* **72**, 399 (1947).
 [6] J. E. Turner, *American Journal of Physics* **45**, 758 (1977).

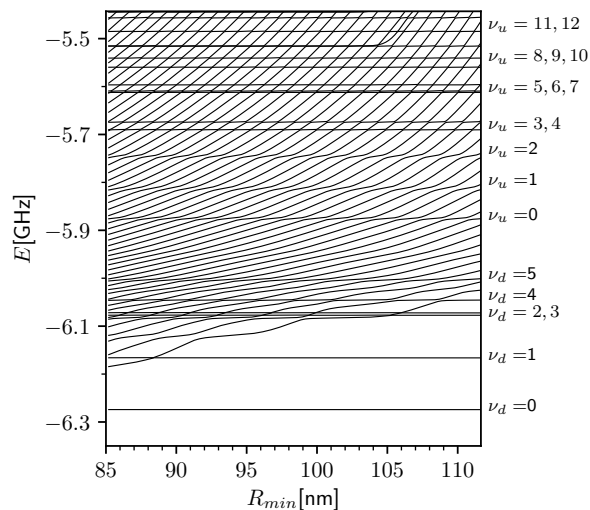


FIG. 8. For the two bound states of the electronics states of Cs-RbCs Rydberg molecule $\text{Cs}(42s)\text{-RbCs}(N = 2)$ and $\text{Cs}(38f)\text{-RbCs}(N = 1)$ presented in Fig. 3 (a), stabilization diagram of the energies as a function of the lower minimum value of the radial coordinate R_{min} used in the numerical method to solve the coupled Schrödinger equation (8). The vibrational quantum number ν_d of the bound states is indicated in the right axis.

- [7] A. Guttridge, D. K. Ruttley, A. C. Baldock, R. González-Férez, H. R. Sadeghpour, C. S. Adams, and S. L. Cornish, *Phys. Rev. Lett.* **131**, 013401 (2023).
- [8] J. Tallant, S. T. Rittenhouse, D. Booth, H. R. Sadeghpour, and J. P. Shaffer, *Phys. Rev. Lett.* **109**, 173202 (2012).
- [9] D. Booth, S. T. Rittenhouse, J. Yang, H. R. Sadeghpour, and J. P. Shaffer, *Science* **348**, 99 (2015).
- [10] M. Peper and J. Deiglmayr, *Phys. Rev. Lett.* **126**, 013001 (2021).
- [11] R. González-Férez, S. T. Rittenhouse, P. Schmelcher, and H. R. Sadeghpour, *J. Phys. B: At., Mol. Opt. Phys.* **53**, 074002 (2020).
- [12] R. Srikumar, F. Hummel, and P. Schmelcher, *Phys. Rev. A* **108**, 012809 (2023).
- [13] A. Duspayev, A. Shah, and G. Raithel, *New Journal of Physics* **24**, 053043 (2022).
- [14] M. Marinescu, H. R. Sadeghpour, and A. Dalgarno, *Phys. Rev. A* **49**, 982 (1994).
- [15] P. D. Gregory, J. Aldegunde, J. M. Hutson, and S. L. Cornish, *Phys. Rev. A* **94**, 041403 (2016).
- [16] P. K. Molony, P. D. Gregory, Z. Ji, B. Lu, M. P. Köppinger, C. R. Le Sueur, C. L. Blackley, J. M. Hutson, and S. L. Cornish, *Phys. Rev. Lett.* **113**, 255301 (2014).
- [17] E. Fermi, *Il Nuovo Cimento* **11**, 157 (1934).
- [18] H. R. Sadeghpour, Ultracold rydberg atom-atom interaction, in *Springer Handbook of Atomic, Molecular, and Optical Physics*, edited by G. W. F. Drake (Springer International Publishing, Cham, 2023) pp. 795–803.
- [19] U. Fano and A. Rau, in *Atomic Collisions and Spectra*, edited by U. Fano and A. Rau (Academic Press, 1986) pp. 61–80.
- [20] J. Eaton, H. Sarkas, S. Arnold, K. McHugh, and K. Bowen, *Chemical Physics Letters* **193**, 141 (1992).
- [21] W. Domcke, D. R. Yarkony, and H. Köppel, *Conical Intersections* (World Scientific, 2011).
- [22] A. U. Hazi and H. S. Taylor, *Phys. Rev. A* **1**, 1109 (1970).
- [23] E. Kuznetsova, S. T. Rittenhouse, H. R. Sadeghpour, and S. F. Yelin, *Phys. Chem. Chem. Phys.* **13**, 17115 (2011).
- [24] E. Kuznetsova, S. T. Rittenhouse, H. R. Sadeghpour, and S. F. Yelin, *Phys. Rev. A* **94**, 032325 (2016).
- [25] K. Gawlas and S. D. Hogan, *J. Phys. Chem. Lett.* **11**, 83 (2020).
- [26] S. Patsch, M. Zeppenfeld, and C. P. Koch, *J. Phys. Chem. Lett.* **13**, 10728 (2022).
- [27] K. Wang, C. P. Williams, L. R. B. Picard, N. Y. Yao, and K.-K. Ni, *PRX Quantum* **3**, 030339 (2022).
- [28] C. Zhang and M. R. Tarbutt, *PRX Quantum* **3**, 030340 (2022).
- [29] J. Deiglmayr, A. Grochola, M. Repp, K. Mörtlbauer, C. Glück, J. Lange, O. Dulieu, R. Wester, and M. Weidemüller, *Phys. Rev. Lett.* **101**, 133004 (2008).
- [30] W. B. Cairncross, J. T. Zhang, L. R. B. Picard, Y. Yu, K. Wang, and K.-K. Ni, *Phys. Rev. Lett.* **126**, 123402 (2021).
- [31] I. Stevenson, A. Z. Lam, N. Bigagli, C. Warner, W. Yuan, S. Zhang, and S. Will, *Phys. Rev. Lett.* **130**, 113002 (2023).
- [32] T. Takekoshi, L. Reichsöllner, A. Schindewolf, J. M. Hutson, C. R. Le Sueur, O. Dulieu, F. Ferlaino, R. Grimm, and H.-C. Nägerl, *Phys. Rev. Lett.* **113**, 205301 (2014).
- [33] M. Gröbner, P. Weinmann, F. Meinert, K. Lauber, E. Kirilov, and H.-C. Nägerl, *Journal of Modern Optics* **63**, 1829 (2016).
- [34] R. González-Férez, M. Weidemüller, and P. Schmelcher, *Phys. Rev. A* **76**, 023402 (2007).